The Role of Self-Organized TiO 2 Nanotube Thickness on the Electrochemical Performance of Anodes for Li-Ion Microbatteriess

Clement Ghigo, Hanna Sopha, Marcela Sepúlveda, Ludek Hromadko, Jhonatan Rodriguez-Pereira, Florence Vacandio, Killian Dénoue, Jan Macak, Thierry Djenizian

The Role of Self-Organized TiO_2 Nanotube Thickness on the Electrochemical Performance of Anodes for Li-Ion Microbatteriess

*Clement Ghigo, Hanna Sopha, Marcela Sepúlveda, Ludek Hromadko, Jhonatan Rodriguez-Pereira, Florence Vacandio, Killian Dénoue, Jan M. Macak, and Thierry Djenizian**

Self-organized TiO_2 nanotube (TNT) layers with different thicknesses are prepared by anodization of Ti foils and then characterized by X-ray diffraction (XRD), scanning electron microscopy (SEM), X-ray photoelectron spectroscopy (XPS), and electrochemical techniques to be used as potential anodes for Li-ion microbatteries. Electrochemical behaviors between 1 and 190 µm thick electrodes, which are the thickest ever studied layers as electrode, have been evaluated by cyclic voltammetry (CV) and chronopotentiometry at various kinetics. The highest areal capacity is obtained for TNT layers of 190 µm providing an initial discharge capacity of ≈5.3 mAh cm^{-2} at C/10. At faster kinetics, the ≈80 µm thick TNT layer reveals the best electrochemical behavior by offering 256 µAh cm^{-2} at 5 C and a good stability for 200 cycles at C/5. The influence of the increasing thickness on the electrochemical performance at fast rates can be attributed to the uncomplete reaction of TNT layers with Li ions and the enhancement of the formation of a solid electrolyte interphase. It is also shown that a very thick electrode is not able to sustain long and very fast cycles due to the mechanical deformations occurring during the successive insertion/extraction of Li ions.

1. Introduction

The research and development of integrable power sources have been intensified over the last decade to ensure autonomy of microelectronic devices. The technological approach is mainly based on the miniaturization of batteries and supercapacitors that can provide energy to power low-consumption devices for wearable applications. Particularly, miniaturized energy storage systems like Li-ion microbatteries are currently designed to power various electrical appliances as wireless sensors, micro-controllers, medical monitoring devices, etc. In this context, research efforts mainly focus on the development of thin-film active materials and the design of 3D electrodes that may display remarkable features like flexibility/stretchability.[1,2]

As TiO_2 nanorods,[3–5] amorphous and anatase self-organized TiO_2 nanotube (TNT) layers are able to intercalate reversibly Li ions while offering remarkable properties such as high mechanical stability due to the low volume change during cycling (only 3–4%) and high retention capability. In addition, appealing properties such as reliability, eco-friendliness, and cost-effectiveness make them interesting to be used as anodes for Li-ion batteries.[6–9] Such TNT layers can be produced by anodic oxidation of Ti substrates and consist

C. Ghigo, T. Djenizian
Center of Microelectronics in Provence
Flexible Electronics Department
Mines Saint-Etienne
13541 Gardanne, France
E-mail: thierry.djenizian@emse.fr

C. Ghigo, K. Dénoue
Quartier Notre Dame
Pellenc Energy S.A.S.
Route de Cavaillon, 84120 Pertuis, France

H. Sopha, M. Sepúlveda, L. Hromadko, J. Rodriguez-Pereira, J. M. Macak
Center of Materials and Nanotechnologies
Faculty of Chemical Technology
University of Pardubice
Nam. Cs. Legii 565, 53002 Pardubice, Czech Republic

H. Sopha, L. Hromadko, J. M. Macak
Central European Institute of Technology
Brno University of Technology
Purkyňova 123, 612 00 Brno, Czech Republic

F. Vacandio
CNRS
MADIREL Laboratory
UMR 7246
Aix-Marseille University
13397 Marseille, France

T. Djenizian
Center of Physical-Chemical Methods of Research and Analysis
Al-Farabi Kazakh National University
Tole bi str., 96A., Almaty 050012, Kazakhstan

The ORCID identification number(s) for the author(s) of this article can be found under https://doi.org/10.1002/ente.202400528.

DOI: 10.1002/ente.202400528

of vertically aligned TNTs on the Ti substrate with open nanotube tops.[10,11] The advantages of such TNT layers over other TiO_2 nanostructures for use in Li-ion batteries is their direct contact to the underlying Ti, which can be used as electrical contact,[10] as well as the straight diffusion path for the Li-ions within the nanotubes, resulting in an excellent electrochemical performance.[12]

For the preparation of TNT layers different electrolytes containing a F^- source (such as NH_4F or HF) can be employed, resulting in TNT layers with different thickness and nanotube diameters. In aqueous acidic electrolytes (so-called first-generation electrolytes) TNT layers with thickness up to ≈500 nm and diameters between ≈10 and ≈100 nm can be achieved.[13–15] The fact that such TNT layers are very thin, can be related to a strong etching effect on the nanotube top stemming from the acidity of the electrolytes. In aqueous neutral electrolytes, second-generation electrolytes, slightly thicker TNT layers up to ≈2.5 μm with diameters similar as in aqueous acidic electrolytes can be prepared.[16–18] In such neutral electrolytes, the etching rate on the nanotube top is strongly reduced compared to acidic electrolytes, while the growth rate is approximately the same. In viscous organic electrolytes, the third-generation electrolytes, TNT layers a few μm up to several hundreds of μm can be achieved, while the diameters of the nanotubes produced in such electrolytes can be as large as several hundreds of nm.[19–21] Due to the viscosity, the migration of ions in the organic electrolytes is very low, which reduces the etching rate of the nanotube tops as well as the growth rates of the nanotubes. Therefore, much longer anodization times than in aqueous electrolytes must be applied. Additionally, due to a high IR drop, higher potentials than in aqueous electrolytes must be applied. The exact TNT layer morphology, i.e., TNT layer thickness and nanotube diameter, strongly depends on the electrolyte composition, applied potential and anodization time.

Since 2009, several chemical functionalization methods have been reported to further increase the electrochemical properties of TNT layers.[22] Indeed, TNTs have been successfully modified by doping processes,[23,24] chemical treatments,[25] and thin-coating techniques including electrodeposition[26] and atomic layer deposition (ALD).[27–29] Electrode thickening is an intuitive approach to improve the performance without additionally increasing the electrode fabrication fees.[30,31] Then, self-supported TNT layers thicker than 1 μm have been studied for a specific loading and different size.[32,33] Previous work by González et al. reported that a 50 μm thick TNT layer could deliver an areal discharge capacity of 2 mAh cm^{-2}.[34] However, there is no report on the electrochemical performance of thicker TNT layers so far.

In the present work, we briefly describe the preparation of thickness-controlled TNT layers ranging from 1 to 190 μm. The electrochemical performance of four different thicknesses of TNT layers has been assessed at different kinetics. We report that the thicker the TNT layer, the better the capacity with good stability as long as the cycling rate remains lower than C/2. Actually, the capacity decreases with increasing thickness and C-rate due to different effects: electrode degradation due to the variation of the volume electrode, the diffusion coefficient of Li ions in bulk TNTs combined, and the enhanced formation of a solid electrolyte interphase (SEI).

2. Result and Discussion

Figure 1a shows SEM top-view and cross-sectional images of the four different kinds of TNT layers, i.e., with different thickness and diameter, used as anodes in this study. As one can see, all TNT layers consist of open nanotubes with nominal thickness of 1, 35, 80, and 190 μm. Thickness and diameter of the employed TNT layers are given in **Table 1**. To obtain the nanotube layers with thicknesses over such a wide range, electrolytes of three different compositions had to be employed, namely an glycerol-based electrolyte containing 50 vol% H_2O and a small amount of NH_4F for the 1 μm thick TNT layers,[35] an ethylene glycol-based electrolyte containing small amounts of water and NH_4F for the 35 μm thick TNT layers,[36] and an ethylene glycol-based electrolyte containing small amounts of HF.[21] Due the different electrolyte compositions and different applied potentials optimized for these electrolytes (the main parameters influencing the nanotube diameter of anodic TNT layers), TNT layers possessed different nanotube diameters.[10,11,37] Just the 80 and 190 μm thick TNT layers, which were prepared in the same electrolyte at the same potential, show identical nanotube diameters. It is, however, expected that the nanotube diameter plays a minor role if TNT layers with so distinctly different thicknesses are employed in Li-ion batteries as the significantly increased thickness results in significantly increased space and mass for Li^+ insertion than the comparably small nanotube diameter changes would lead to. The mass of the TiO_2 per cm^2 of the macroscopic electrode area is given in Table 1 and was calculated by determining the porosity of the TNT layers, assuming a nanotube shape of a cylinder and using the density of TiO_2 anatase phase (3.9 g cm^{-3}).

It can be pointed that compared to 1 μm thick layer, more thicker layers show a weaker adhesion to the underlying Ti substrate and tend to peel off during annealing at higher temperatures. Therefore, the 35, 80, and 190 μm thick TNT layers were annealed at 340 °C for 1 h. Figure 1b shows the XRD pattern of the TNT layers with different thickness, verifying their crystallization also at the lower employed annealing temperature.

The influence of thickness was evidenced by EIS in Figure 1c. The semicircle in the medium frequency range is attributed to the impedance due to the charge transfer resistance. The increase of the electrode thickness goes with the increase of the resistivity. The thicker the TiO_2 nanotubes are, the higher the porosity of electrode is, the higher the charge transfer resistance is. However, the increase of the semicircle diameter revealed a rise of the electrode capacity confirming that the thicker TNT layers initially offer more TiO_2 active material.

The first charge/discharge profiles at 0.1 C shown in **Figure 2**a,d exhibit typical behavior of lithium storage in TiO_2 anatase due to the presence of two plateaus at around 1.75 and 1.9 V corresponding to the reversible insertion of Li ions in octahedral vacant sites of TiO_2.[38] This effect is also confirmed by the presence of sharp peaks on the graph reporting the variation of the differential capacity as a function of the potential (see Figure 2b). At C/10, high initial discharge capacity of 5.3 mAh cm^{-2} has been obtained for the 190 μm sample, indicating that ultra-thick electrode is able to insert reversibly Li ions. As intuitively expected, the discharge capacity clearly decreases with thickness lowering 3.1, 1.4, and 0.05 mAh cm^{-2} for the

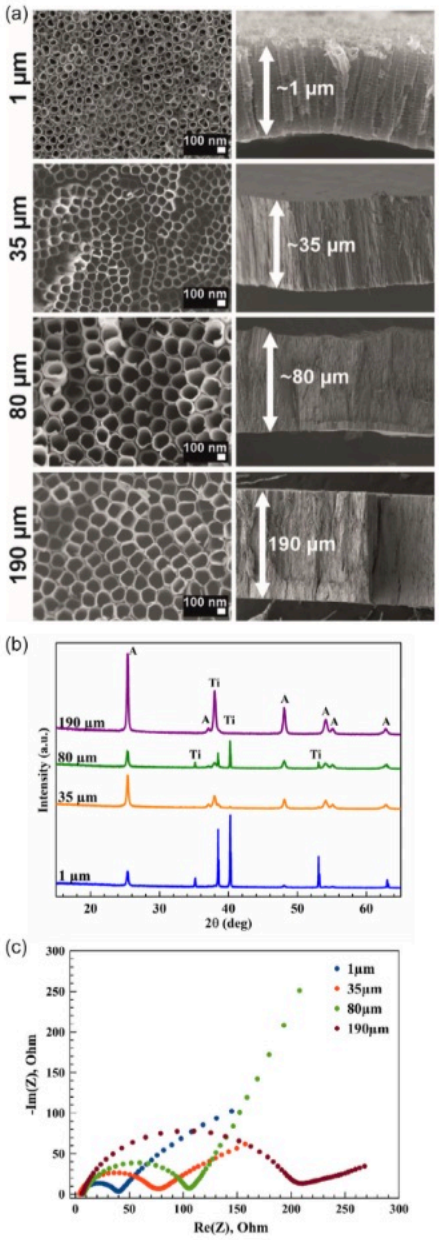

Figure 1. a) SEM top views (left column) and cross-sectional views (right column) of 1, 35, 80, and 190 µm thick TNT layers, and b) XRD pattern of the TNT layers of different thickness annealed at 400 °C (1 µm thick TNT layer) and 340 °C (35, 80, and 190 µm thick TNT layers). A – anatase, Ti – titanium. c) Nyquist plots for 1, 35, 80, and 190 µm thick TNT layers before cycling experiments.

Table 1. Characteristics and annealing conditions of TNT layers.

Nominal thickness [µm]	Measured thickness [µm]	Diameter [nm]	Calculated mass of TiO_2 [cm^2]	Annealing temperature [°C]
1	1.2 ± 0.17	82.2 ± 10.6	≈0.109 mg	400
35	35.6 ± 0.6	109.3 ± 12.1	≈2.1 mg	340
80	78.4 ± 18.9	181.1 ± 20.9	≈4.33 mg	340
190	190.6 ± 9.3	170.1 ± 25.1	≈15.97 mg	340

80, 35, and 1 µm samples, respectively. Evolution of the discharge capacity during 10 cycles at C/10 in Figure 2c reveals a very good stability from the 2nd cycle while a strong fading occurs after the 1st discharge that can be attributed to the SEI formation (discussed in more details later).

Discharge capacity stability of the four different thick TNT layers has been evaluated for 200 cycles at a rate of C/5 (See **Figure 3**). As shown in Figure 3a the capacity retention is improved with the increasing electrode thickness while the first irreversible discharge capacity tends to increase suggesting that SEI growth is promoted for longer nanotubes. The best performance is obtained for the 190 µm TNT layer that delivers the highest capacity values ranging from 4.25 mAh cm^{-2} at the 1st cycle to 3.2 mAh cm^{-2} at the 50th cycle and can retain 74% of the initial discharge capacity. However, a strong continuous capacity fading occurs for longer cycles and areal capacity tends to stabilize at 0.5 mAh cm^{-2} after 125 cyles. This effect can be attributed to the volume variations of the TNT layers during the successive charge/discharge processes leading to mechanical strains responsible for the electrode damaging. Although the volume expansion of TiO_2 anatase is low (around 4%), the very thick electrode is more subjected to degradation during the reversible insertion of Li ions. Actually, the very thick electrode becomes more brittle and can be easily detached from the substrate, and therefore is not able to sustain long cycling tests. Finally, the 80 µm thick layer shows the best cycling properties as it can deliver 1.25 mAh cm^{-2} at the 200th cycle.

Electrochemical performance of different TNT layers at various kinetics for 70 cycles are shown in **Figure 4** and main characteristics obtained from the curves are listed in **Table 2**. Except for the thickest TNT layer, stable discharge capacities are observed for 60 cycles at various kinetics varying from C/10 to 5 C. It can be noted that capacities are retrieved after the 60th cycle at C/5 confirming good electrochemical behaviors. Compared to other thicknesses, the 190 µm thick TNT layer reveals the best performance up to C/2. But at faster kinetics, huge capacity fading occurs leading to poor electrochemical features. Indeed, an irreversible drop of capacity is registered during discharge tests at 1 C leading to a 77% loss of the initial capacity at the 40th cycle. In addition, only 0.001% of the initial capacity is retained at 5 C and discharge capacity cannot be retrieved after the 60th at C/5 suggesting that fast cycling strongly affects the electrode capability. This poor performance is confirmed by the very low capacity retrieved after 60 cycles at C/5. More remarkably, the capacity at 5 C becomes even smaller than that obtained from the thinnest layer. This behavior can be also explained by

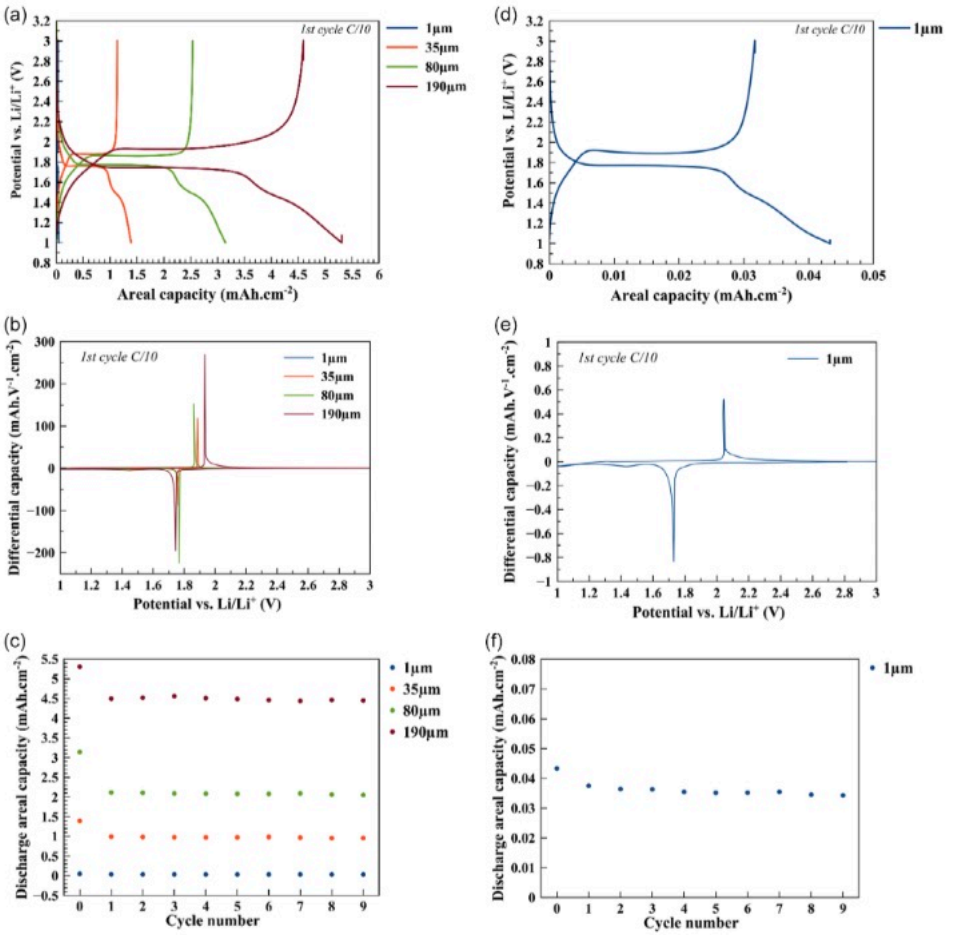

Figure 2. a) First charge–discharge capacities at C/10 of 1, 35, 80, and 190 µm thick TNT layers, b) corresponding differential capacity versus potential, c) variation of the discharge capacity for 10 cycles, and d–f) graphs plotted for the 1 µm thick layer.

the mechanical deformations occurring during the cycling tests. It is also apparent that high kinetics are responsible for fast structural changes enhancing mechanical damage that cannot be endured by the very thick electrode.

In order to have a better insight into the TNT's electrochemical performance, the evolution of the first discharge capacity *vs* electrode thickness at different kinetics has been plotted and is shown in **Figure 5**a. The linear behaviours observed for low kinetics ranging from C/10 to C/2 reveal that the capacity values are proportional to the electrode thickness. This result confirms that the Li^+ insertion/extraction process occurs in a similar manner along the nanotubes leading to a gained capacity proportional to the electrode thickness. When the rate attains C, the linear behaviour evolves into a polynomial dependence. At this stage, the curves reach a maximum peak indicating a threshold value of nanotube thickness for getting the optimal capacity. It can be pointed out that the results are in good agreement with the non-linear relationship between the delivered capacity and the NTs length reported by González et al.[34] Such an unexpected effect suggests a modification of the Li ion reactions with TNTs under high applied currents. Thus, the best performance at very fast kinetic (5 C) is achieved by the 80 µm nanotubes in length.

To better understand the electrode behaviours at fast kinetics, the thickness-normalized discharge areal capacity has been assessed and displayed in Figure 5b. As it can be predicted, the capacity decreases with the cycling rate but also decreases continuously with the electrode thickness suggesting that diffusion of Li ions might be also responsible for the capacity fading of

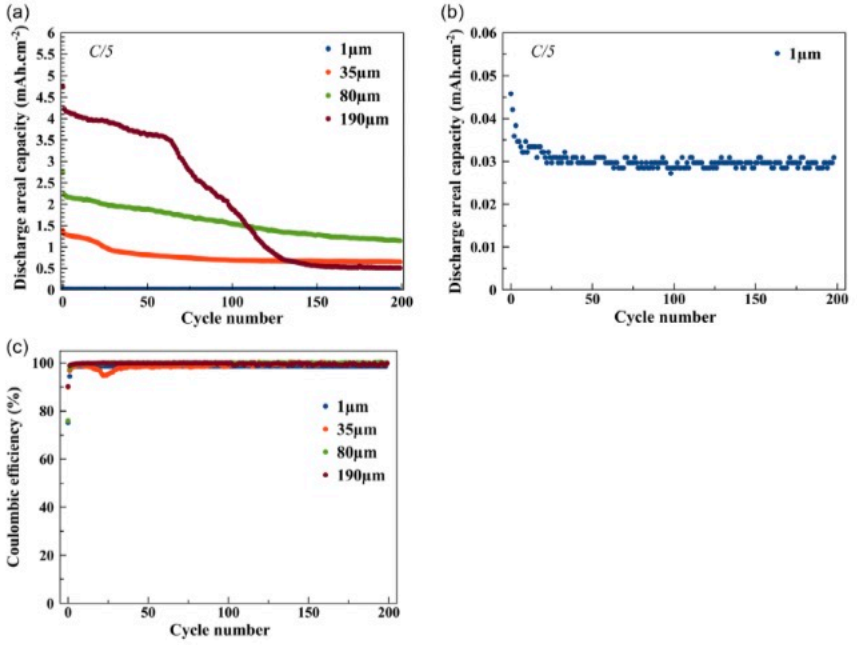

Figure 3. a) Evolution of the discharge capacities for different thick TNT layers at C/5 for 200 cycles. b) Graph plotted for the 1 µm thick layer. c) Coulombic efficiency for different TNT layers at C/5.

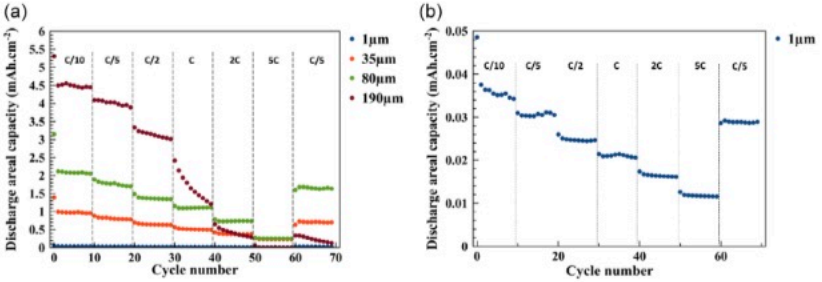

Figure 4. a) Electrochemical performance of different four different thick TNT layers at various C-rates for 70 discharge cycles and b) graph plotted for the 1 µm thick layer.

thicker electrodes at fast kinetics. Indeed, the coefficient diffusion of Li^+ would not be high enough to ensure the complete lithiation/delithiation reactions of the thickest layers and this effect is even stronger with increasing C-rates.

CV tests at different scan rates have been performed to study the evolution of the coefficient diffusion of Li ions in different TNT layers, - see **Figure 6**. All redox peaks are in line with the peaks of the differential capacities observed in Figure 2b, e, which is consistent with the reversible insertion of Li^+ in anatase that occurs according to Equation (1).

$$Li^+ + TiO_2 + xe^- \rightleftarrows Li_xTiO_2 \quad (x = 0.5) \tag{1}$$

Clearly, decreasing of the normalized current density with the TNT layer thickness confirms results obtained from chronopotentiometry experiments.

From the CVs, it is possible to calculate the diffusion coefficient of Li^+ at room temperature using the Randles–Sevcik Equation (2)

$$I_p = 268600n^{3/2}AD^{1/2}Cn^{1/2} \tag{2}$$

Table 2. Main electrochemical characteristics. DC – discharge capacity and ICR – initial capacity retention.

Rate	Cycle #	Electrochemical characteristics	1 µm	35 µm	80 µm	190 µm
C/10	1	DC [µAh cm^{-2}]	50	1391	3143	5305
		DC [µAh cm^{-2} µm^{-1}]	50	40	40	28
		DC [mAh g^{-1}]	459	662	726	332
	2	DC [µAh cm^{-2}]	38	993	2113	4496
		DC [µAh cm^{-2} µm^{-1}]	38	28	26	24
		DC [mAh g^{-1}]	349	473	488	282
		ICR [%]	76	71	67	85
C/5	12	DC [µAh cm^{-2}]	30	836	1831	4070
		DC [µAh cm^{-2} µm^{-1}]	30	24	23	21
		DC [mAh g^{-1}]	275	398	423	255
		ICR [%]	61	60	58	77
C/2	22	DC [µAh cm^{-2}]	25	664	1391	3203
		DC [µAh cm^{-2} µm^{-1}]	25	19	17	17
		DC [mAh g^{-1}]	229	316	321	201
		ICR [%]	51	48	44	60
C	32	DC [µAh cm^{-2}]	21	529	1095	1939
		DC [µAh cm^{-2} µm^{-1}]	21	15	14	10
		DC [mAh g^{-1}]	193	252	253	121
		ICR [%]	43	38	35	37
2 C	42	DC [µAh cm^{-2}]	17	393	734	491
		DC [µAh cm^{-2} µm^{-1}]	17	11	9	3
		DC [mAh g^{-1}]	156	187	170	31
		ICR [%]	35	28	23	9
5 C	52	DC [µAh cm^{-2}]	12	241	256	5
		DC [µAh cm^{-2} µm^{-1}]	12	7	3	0
		DC [mAh g^{-1}]	11	115	59	0.3
		ICR [%]	24	17	8	0
C/5	62	DC [µAh cm^{-2}]	29	729	1678	305
		DC [µAh cm^{-2} µm^{-1}]	29	21	21	2
		DC [mAh g^{-1}]	266	347	388	19
		ICR [%]	58	52	53	6

where I_p is the peak current, n is the number of electrons involved in the redox reaction of Ti^{3+}/Ti^{4+} which is equal to 0.5, A is the electrode surface area (active surface area of TNTs) which is ≈150 cm^2 µm^{-1}, D is the diffusion coefficient of Li^+, and C is the maximum concentration of Li^+ (or Ti^{3+}) in the lattice (0.024 mol cm^{-3} at $x = 0.5$).

Diffusion coefficients of Li ions given in **Table 3** have been calculated from cathodic peaks recorded at 1 and 0.25 mV s^{-1}. First, it is worth to mention that the diffusion coefficient values of Li^+ in bulk anatase are consistent with other works.[38] Then, it is clearly apparent that the diffusion coefficient decreases when the thickness of TNT increases. In addition, faster cycling rate does not affect the diffusion coefficient obtained from TNTs up to 35 µm thick but this tendency is not verified for thicker layers. Indeed, from the 80 µm TNT layer, the longer TNTs the lower diffusion coefficient confirming the previous assumption. In fact, the evolution of the diffusion coefficient with the TNT thickness can be correlated to the uncomplete reaction of the TNT layers with Li ions and the growth of SEI.

The SEI formation can be highlighted through the evaluation of the storage contributions that can be determined with the exponential values obtained from the equation $I_p = C_1\nu + C_2\nu^{0.5}$.[39] The first term $C_1\nu$ determines the pseudo-capacitive contribution; the second term $C_2\nu^{0.5}$ is referring to the bulk intercalation. **Figure 7** shows the variation of the anodic and cathodic peak currents determined by CV as a function of the scan rate. For all samples, the x value is equal or very close to 0.5 suggesting a typical battery behavior regarding the mode of charge storage. As the thickness increases between the 1 and 35 µm samples, x value rises from 0.51 to 0.60 revealing the slight pseudo-capacitive effect enhancement, which is in line with the increase of the porosity. For 80 and 190 µm samples, x value is equal to 0.5, meaning that Li^+ storage in the bulk is predominant for thicker electrodes while the porosity is strongly increased. The same behavior is noted for the Li^+ extraction as the x value change from 0.58 to 0.65 between 1 and 35 µm while it remains at 0.5 for the 80 and 190 µm thick TNTs. The lowering pseudo-capacitive effect could be attributed to the continuous growth of SEI layer hampering Li^+ storage.

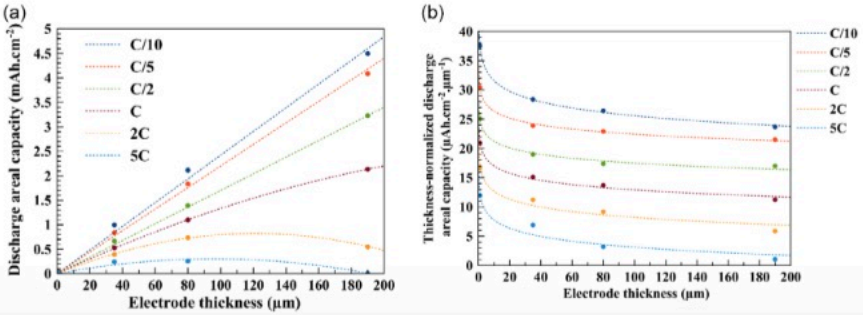

Figure 5. a) Evolution of the 1st discharge capacity and b) the thickness-normalized areal capacity with the TNT thickness at various C-rates.

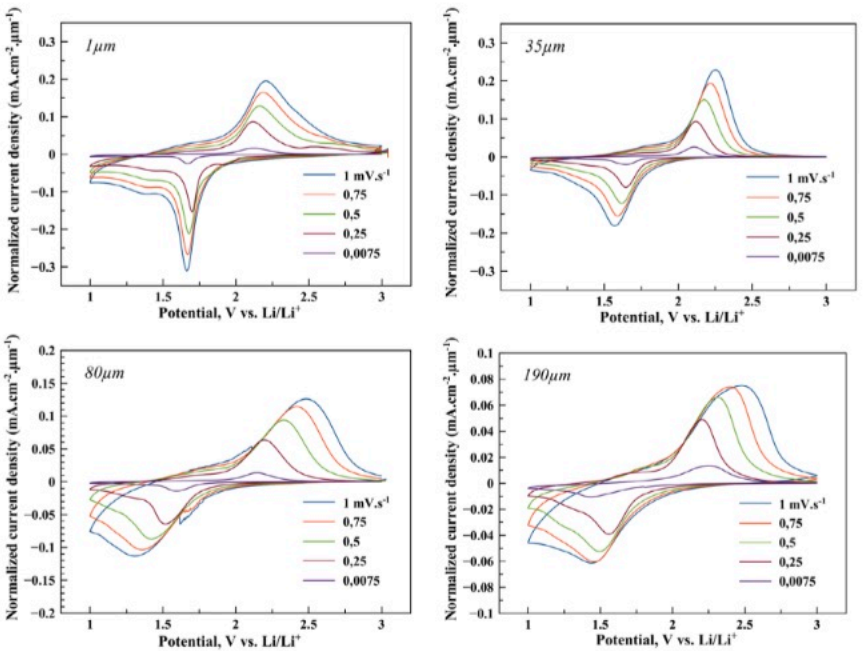

Figure 6. CV tests at various scan rates for TNT layers with different thickness.

Table 3. Evaluation of diffusion coefficient of Li^+ according to the Randles–Sevcik equation.

Thickness [μm]	1	35	80	190
$I_{p,1}$ [mA] @ 1 mV s^{-1}	0.3×10^{-3}	6.3×10^{-3}	8.8×10^{-3}	11.4×10^{-3}
$I_{p,0.25}$ [mA] @ 0.25 mV s^{-1}	0.15×10^{-3}	2.8×10^{-3}	5.2×10^{-3}	7.6×10^{-3}
D_1 [cm^2 s^{-1}] @ 1 mV s^{-1}	7.69×10^{-16}	2.77×10^{-16}	1.03×10^{-16}	0.31×10^{-16}
$D_{0.25}$ [cm^2 s^{-1}] @ 0.25 mV s^{-1}	7.69×10^{-16}	2.77×10^{-16}	1.45×10^{-16}	0.55×10^{-16}
$D_1/D_{0.25}$	1	1	0.71	0.56

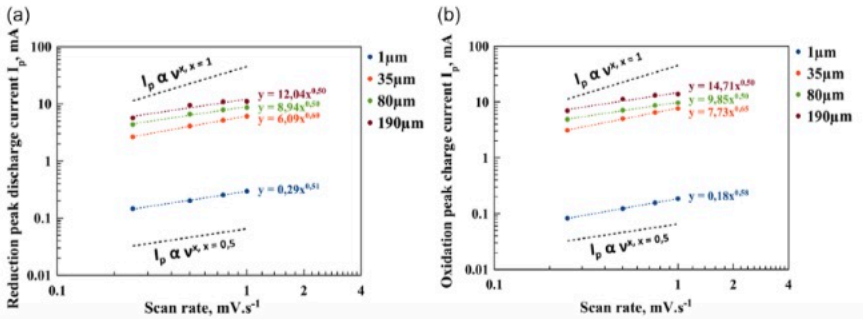

Figure 7. a) Reduction and b) oxidation peak currents versus scan rate plot.

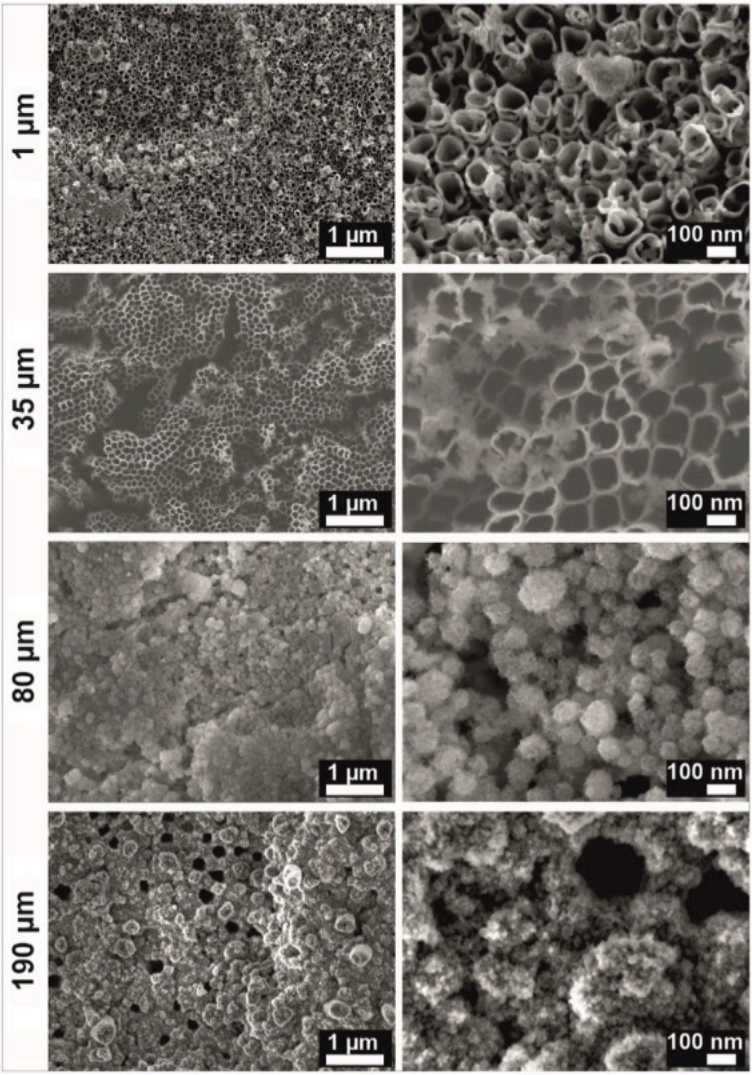

Figure 8. SEM images of 1, 35, 80 and 190 µm TNT layers after cycling experiments. The left column shows low magnification images, the right column shows high magnification images.

Post-mortem analyses have been performed to corroborate the data obtained from electrochemical experiments. First, SEM images of different thickness TNT layers are shown in **Figure 8**. Clearly, 80 and 190 µm samples reveal the presence of a rather thick SEI layer on top (difficult to remove away by post-mortem washing, compared to the thinner TNT layers), explaining the exclusive bulk diffusion of Li^+ into very thick electrodes due to the clogging of nanotubes. The SEI formation seems to be promoted for the thickest TNT layers.

Figure 9 shows post-cycling XRD and XPS analysis of 1, 35, 80, and 190 µm samples. Same elements have been detected between electrodes regardless their thickness. These results confirm that no other chemical modification of nanotubes occurred after cycling tests except for the SEI formation, which is definitely confirmed by the increase of the F signal with the increasing layer thickness. Indeed, the longer nanotubes, the higher amount of F incorporation leading to the probable enhanced formation of LiF.

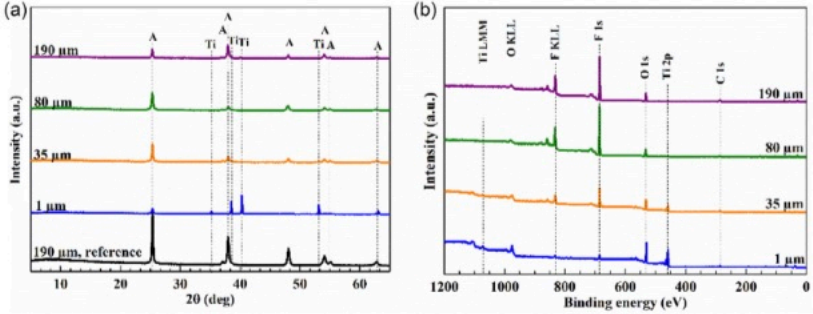

Figure 9. a) Post-mortem XRD and b) XPS analysis for TNT layers used in this work. The XRD pattern of the 190 µm reference sample (representing an unused TNT layer) is also included.

3. Conclusion

To summarize, the discharge capacity increases linearly with the TNT layer thickness as long as the C-rate remains below 1 C. The best performance has been obtained for the 190 µm TNT layer that reached 5.3 mAh cm^{-2} at C/10. Such a very thick layer could also deliver the highest capacity values at C/5 ranging from 4.25 mAh cm^{-2} at the 1st cycle and can retain 74% of the initial discharge capacity for 50 cycles. However, study performed at faster kinetics up to 5 C and longer cycles (>70) showed that the best performance is achieved by the 80 µm thick nanotubes layers. Indeed, an irreversible capacity loss of the 190 µm thick occurred due to mechanical deformations during the cycling tests while the 80 µm is able to retrieve the capacity after 60 cycles. A better insight into the electrochemical behaviour by CV investigations revealed that the diffusion coefficient of Li^+ decreases with the increasing TNT thickness suggesting that the reversible insertion reaction does not occur all along the nanotubes. In addition, we showed that the SEI formation is promoted for a thicker TNT layer.

4. Experimental Section

TNT Layer Preparation: TNT layers were synthesized by an anodization process. ≈1 µm thick TNT layers were prepared in a glycerol-based electrolyte containing 270 mM NH_4F and 50 vol% H_2O at 20 V for 100 min.[35] 35 µm thick TNT layers were prepared in an ethylene glycol-based electrolyte (aged for 9 h)[40] containing 170 mM NH_4F and 3 vol% H_2O at 60 V for 4 h.[36] 80 and 190 µm thick TNT layers were prepared in an ethylene glycol-based electrolyte containing 0.2 M HF (40%) at 140 V for 4 and 16 h, respectively.[21] As as-prepared TNT layers are amorphous, 1 µm thick TNT layers were annealed at 400 °C and the thicker layers at 340 °C in a muffle for 1 h (heating rate: 2.1 °C min^{-1}) to receive anatase phase. The lower annealing temperature for the thicker TNT layers was chosen to avoid a lifting-off of the TNT layers from the underlying Ti substrate.

Battery Preparation and Characterization: Electrodes were put under vacuum overnight prior to cell assembly. Two-electrode Swagelok type cells were used for assembling electrodes from 1 µm to 80 µm thick in half-cell configuration. A stainless-steel split flat cell (MTI Corporation) was preferred for cycling thicker anodes. This setup turned out to be necessary to avoid the cutting of samples and prevent mechanical degradation. The organic liquid electrolyte was based on $LiPF_6$ salts dispersed in carbonate solvents (ethylene carbonate:dimethyl carbonate [1:1]). A metallic lithium foil was used as counter and reference electrode to complete the cell while a Whatman glass microfiber paper embedded by the electrolyte was selected as separator. Galvanostatic charge–discharge tests were carried out at room temperature with a Biologic potentiostat VMP and a galvanostatic cycling with potential limitation technique (GCPL). The chronopotentiometry tests were performed at different kinetics in a 1–3 V voltage window versus Li/Li^+. Electrochemical performance tests were carried out at C-rates ranging from C/10 to 5 C. An initial open-circuit relaxation of 24 h was imposed for Split Cell tests to reach a steady-state. Cyclic voltammetry (CV) and electrochemical impedance spectroscopy (EIS) were privileged for a better understanding of the electrochemical behaviors. CV curves were obtained at various scan rates of 0.25, 0.5, 0.75, and 1 mV s^{-1} between 1 and 3 V versus Li/Li^+. EIS measurements were conducted at open circuit voltage over frequencies ranging from 200 kH to 10 mHz with a sine modulation of 10 mV.

Material Characterization: The morphology of the TNT layers was examined using a field-emission scanning electron microscope (FE-SEM, JEOL JSM 7500F). Dimensions of the TNT layers were evaluated using proprietary Nanomeasure software. A minimum of 85 diameter and 17 cross-section measurements were used to assess diameter and thickness of the TNT layers. All measurements are given as average ± standard deviation (SD). For an easier overview, all TNT layers are named by their nominal thickness within this study. To investigate the structure of the TNT layers, X-ray diffraction (XRD, PANanalytical Empyrean diffractometer) equipped with a Cu X-ray tube and a scintillation detector Pixcel[3D] was used at 45 kV in the 2θ range of 5–70°. X-ray photoelectron spectroscopy (XPS) (XPS, ESCA2SR, Scienta-Omicron) equipped with a monochromatic Al Kα (1486.7 eV) source was used to investigate the surface chemical composition of the post-mortem TNT layers. The binding energy scale was referenced to adventitious carbon ($E_B = 284.8$ eV). Quantification was carried out using the sensitivity factors provided by the manufacturer. The data analysis was conducted in CasaXPS software.

Acknowledgements

C.G. and H.S. contributed equally to this work. The authors acknowledge Institut Mines Telecom, Ecole des Mines de Saint-Etienne, the Ministry of Education, Youth and Sports of the Czech Republic for supporting CEMNAT (LM2023037) infrastructure providing SEM, EDX, XPS and XRD accesses.

Conflict of Interest

The authors declare no conflict of interest.

Data Availability Statement

The data that support the findings of this study are available from the corresponding author upon reasonable request.

Keywords

anodes, energy storage, Li-ion microbatteries, TiO_2 nanotubes

Received: March 21, 2024
Revised: May 28, 2024
Published online: July 20, 2024

[1] M. Nasreldin, S. de Mulatier, R. Delattre, M. Ramuz, T. Djenizian, *Adv. Mater. Technol.* **2020**, *5*, 2000412.
[2] S. Mukherjee, A. Albertengo, T. Djenizian, *Energy Storage Mater.* **2021**, *42*, 773.
[3] X. Han, X. Han, L. Sun, P. Wang, M. Jin, X.-J. Wang, *Mater. Chem. Phys.* **2016**, *171*, 11.
[4] N. Kitchamsetti, R. S. Kalubarme, P. R. Chikate, C.-J. Park, Y.-R. Ma, P. M. Shirage, R. S. Devan, *ChemistrySelect* **2019**, *4*, 6620.
[5] S. Dong, H. Wang, L. Gu, X. Zhou, Z. Liu, P. Han, Y. Wang, X. Chen, G. Cui, L. Chen, *Thin Solid Films* **2011**, *519*, 5978.
[6] D. Fang, K. Huang, S. Liu, Z. Li, *J. Alloys Compd.* **2008**, *464*, L5.
[7] G. F. Ortiz, I. Hanzu, T. Djenizian, P. Lavela, J. L. Tirado, P. Knauth, *Chem. Mater.* **2009**, *21*, 63.
[8] T. Djenizian, I. Hanzu, P. Knauth, *J. Mater. Chem.* **2011**, *21*, 9925.
[9] B. L. Ellis, P. Knauth, T. Djenizian, *Adv. Mater.* **2014**, *26*, 3368.
[10] J. M. Macak, H. Tsuchiya, A. Ghicov, K. Yasuda, R. Hahn, S. Bauer, P. Schmuki, *Curr. Opin. Solid State Mater. Sci.* **2007**, *11*, 3.
[11] K. Lee, A. Mazare, P. Schmuki, *Chem. Rev.* **2014**, *114*, 9385.
[12] H. Han, T. Song, E. K. Lee, A. Devadoss, Y. Jeon, J. Ha, Y. C. Chung, Y. M. Choi, Y. G. Jung, U. Paik, *ACS Nano* **2012**, *6*, 8308.
[13] M. Assefpour-Dezfuly, C. Vlachos, E. H. Andrews, *J. Mater. Sci.* **1984**, *19*, 3626.
[14] D. Gong, C. A. Grimes, O. K. Varghese, W. Hu, R. S. Singh, Z. Chen, E. C. Dickey, *J. Mater. Res.* **2011**, *16*, 3331.
[15] R. Beranek, H. Hildebrand, P. Schmuki, *Electrochem. Solid-State Lett.* **2003**, *6*, B12.
[16] A. Ghicov, H. Tsuchiya, J. M. Macak, P. Schmuki, *Electrochem. Commun.* **2005**, *7*, 505.
[17] J. M. Macak, K. Sirotna, P. Schmuki, *Electrochim. Acta* **2005**, *50*, 3679.
[18] J. M. Macak, H. Tsuchiya, P. Schmuki, *Angew. Chem., Int. Ed.* **2005**, *44*, 2100.
[19] J. M. Macak, H. Tsuchiya, L. Taveira, S. Aldabergerova, P. Schmuki, *Angew. Chem., Int. Ed.* **2005**, *44*, 7463.
[20] J. M. Macak, P. Schmuki, *Electrochim. Acta* **2006**, *52*, 1258.
[21] S. P. Albu, A. Ghicov, J. M. Macak, P. Schmuki, *Phys. Status Solidi RRL* **2007**, *1*, R65.
[22] V. Galstyan, J. M. Macak, T. Djenizian, *Appl. Mater. Today* **2022**, *29*, 101613.
[23] Z. Lu, C. T. Yip, L. Wang, H. Huang, L. Zhou, *ChemPlusChem* **2012**, *77*, 991.
[24] H. Sopha, C. Ghigo, S. Ng, M. Alijani, L. Hromadko, J. Michalicka, T. Djenizian, J. M. Macak, *Mater. Chem. Phys.* **2022**, *276*, 125337.
[25] G. D. Salian, M. Krbal, H. Sopha, C. Lebouin, M. V. Coulet, J. Michalicka, L. Hromadko, A. T. Tesfaye, J. M. Macak, T. Djenizian, *Appl. Mater. Today* **2019**, *16*, 257.
[26] G. D. Salian, C. Lebouin, A. Demoulin, M. S. Lepihin, S. Maria, A. K. Galeyeva, A. P. Kurbatov, T. Djenizian, *J. Power Sources* **2017**, *340*, 242.
[27] H. Sopha, G. D. Salian, R. Zazpe, J. Prikryl, L. Hromadko, T. Djenizian, J. M. Macak, *ACS Omega* **2017**, *2*, 2749.
[28] A. T. Tesfaye, H. Sopha, A. Ayobi, R. Zazpe, J. Rodriguez-Pereira, J. Michalicka, L. Hromadko, S. Ng, Z. Spotz, J. Prikryl, J. M. Macak, T. Djenizian, *Nanomaterials* **2020**, *10*, 953.
[29] H. Sopha, A. T. Tesfaye, R. Zazpe, J. Michalicka, F. Dvorak, L. Hromadko, M. Krbal, J. Prikryl, T. Djenizian, J. M. Macak, *FlatChem* **2019**, *17*, 100130.
[30] M. Singh, J. Kaiser, H. Hahn, *J. Electrochem. Soc.* **2015**, *162*, A1196.
[31] Y. Kuang, C. Chen, D. Kirsch, L. Hu, *Adv. Energy Mater.* **2019**, *9*, 1901457.
[32] W. Wei, G. Oltean, C. W. Tai, K. Edström, F. Björefors, L. Nyholm, *J. Mater. Chem. A* **2013**, *1*, 8160.
[33] J. Zou, G. Wu, W. Jiang, C. Bao, J. Zou, *J. New Mater. Electrochem.* **2020**, *23*, 280.
[34] J. R. González, R. Alcántara, F. Nacimiento, G. F. Ortiz, J. L. Tirado, E. Zhecheva, R. Stoyanova, *J. Phys. Chem. C* **2012**, *116*, 20182.
[35] S. Das, H. Sopha, M. Krbal, R. Zazpe, V. Podzemna, J. Prikryl, J. M. Macak, *ChemElectroChem* **2017**, *4*, 495.
[36] R. Zazpe, M. Knauth, H. Sopha, L. Hromadko, M. Albert, J. Prikryl, V. Gärtnerová, J. W. Bartha, J. M. Macak, *Langmuir* **2016**, *32*, 10551.
[37] D. Regonini, C. R. Bowen, A. Jaroenworaluck, R. Stevens, *Mater. Sci. Eng.: R: Rep.* **2013**, *74*, 377.
[38] N. Plylahan, A. Demoulin, C. Lebouin, P. Knauth, T. Djenizian, *RSC Adv.* **2015**, *5*, 28474.
[39] B. Laskova, M. Zukalova, A. Zukal, M. Bousa, L. Kavan, *J. Power Sources* **2014**, *246*, 103.
[40] H. Sopha, L. Hromadko, K. Nechvilova, J. M. Macak, *J. Electroanal. Chem.* **2015**, *759*, 122.